New Journal of Physics
The open access journal at the forefront of physics

Deutsche Physikalische Gesellschaft DPG IOP Institute of Physics

OPEN ACCESS

Focusing a deterministic single-ion beam

To cite this article: Wolfgang Schnitzler *et al* 2010 *New J. Phys.* **12** 065023

View the article online for updates and enhancements.

Related content

- Transport of ions in a segmented linear Paul trap in printed-circuit-board technology
G Huber, T Deuschle, W Schnitzler et al.
- Sideband cooling and coherent dynamics in a microchip multi-segmented ion trap
Stephan A Schulz, Ulrich Poschinger, Frank Ziesel et al.
- Demonstration of integrated microscale optics in surface-electrode ion traps
J True Merrill, Curtis Volin, David Landgren et al.

Recent citations

- Trapping, shaping, and isolating of an ion Coulomb crystal via state-selective optical potentials
Pascal Weckesser *et al*
- An Overview on the Formation and Processing of Nitrogen-Vacancy Photonic Centers in Diamond by Ion Implantation
Ariful Haque and Sharaf Sumaiya
- Deterministic doping
David N. Jamieson *et al*

This content was downloaded from IP address 141.51.197.22 on 28/05/2021 at 17:17

New Journal of Physics
The open-access journal for physics

Focusing a deterministic single-ion beam

Wolfgang Schnitzler[1,3], Georg Jacob[1], Robert Fickler[2], Ferdinand Schmidt-Kaler[1] and Kilian Singer[1]

[1] Institut für Quanteninformationsverarbeitung, Universität Ulm, Albert-Einstein-Allee 11, D-89069 Ulm, Germany
[2] Institut für Quantenoptik, Quantennanophysik und Quanteninformation, Universität Wien, Boltzmanngasse 5, A-1090 Wien, Austria
E-mail: wolfgang.schnitzler@uni-ulm.de

New Journal of Physics **12** (2010) 065023 (14pp)
Received 30 November 2009
Published 28 June 2010
Online at http://www.njp.org/
doi:10.1088/1367-2630/12/6/065023

Abstract. We focus down an ion beam consisting of single $^{40}Ca^{+}$ ions to a spot size of a few micrometers using an einzel lens. Starting from a segmented linear Paul trap, we have implemented a procedure that allows us to deterministically load a predetermined number of ions by using the potential shaping capabilities of our segmented ion trap. For single-ion loading, an efficiency of 96.7(7)% has been achieved. These ions are then deterministically extracted out of the trap and focused down to a 1σ-spot radius of (4.6 ± 1.3) μm at a distance of 257 mm from the trap center. Compared to previous measurements without ion optics, the einzel lens is focusing down the single-ion beam by a factor of 12. Due to the small beam divergence and narrow velocity distribution of our ion source, chromatic and spherical aberration at the einzel lens is vastly reduced, presenting a promising starting point for focusing single ions on their way to a substrate.

[3] Author to whom any correspondence should be addressed.

© IOP Publishing Ltd and Deutsche Physikalische Gesellschaft

Contents

1. Motivation

In the age of electronic data processing, the demand for more powerful and faster computers is paramount. As already stated by Gordon E Moore in 1965, the number of transistors that can be placed inexpensively on an integrated circuit has increased exponentially, doubling approximately every two years. The miniaturization of semiconductor devices has reached length scales of a few tens of nanometers, where statistical Poissonian fluctuations in the number of doping atoms in a single transistor significantly affect the characteristic properties of the device, e.g. gate voltage or current amplification. Especially when thinking about future solid state quantum processors, statistical fluctuations of the dopant concentration are fatal for systems that are based on single implanted qubit carriers, like color centers in diamond or phosphorus dopants in silicon [1]–[4]. Until recently, most implantation techniques resorted to thermal sources, where control of the number of doping atoms is possible only via a postdetection of the implantation event. However, although a wide range of postdetection schemes (e.g. the observation of Auger electrons, the generation of electron–hole pairs or changes in the conductance of field effect transistors) are available [5]–[9], most of these techniques require either highly charged ions or high implantation energies, which, as a down side, generate unintentional defects in the host material. Another fabrication method revolves around the structuring of chemically treated Si surfaces. Using a hydrogen-terminated Si surface as the starting point, the tip of a tunneling microscope allows for the removal of single hydrogen atoms, which are then replaced by doping atoms such as phosphorus due to a chemical reactive surface binding [10]–[14]. Although this technique is capable of placing single dopants with sub-nm resolution, the applicability is mainly restricted to specific substrates. In order to circumvent the necessity of any postdetection schemes and to expand the applicability to a wider range of elements, deterministic single-ion sources on the basis of optical lattices [15], magneto-optical [16]–[18] and segmented linear Paul traps [19] have been developed.

Here, we present the experimental set-up to focus down on an ion beam consisting of single $^{40}Ca^{+}$ ions to a spot size of a few μm by utilizing an einzel lens. The single-ion beam is generated by a segmented linear Paul trap that allows us to deterministically extract single ions

on demand [19]–[21]. Due to the small beam divergence and narrow velocity distribution of our single-ion source, chromatic and spherical aberration at the einzel lens is strongly reduced, presenting a promising starting point for focusing single ions on a prospective substrate.

The paper is organized as follows. We first describe in section 2 the experimental setup used for the trapping, imaging and manipulation of $^{40}Ca^{+}$ and this includes a detailed description of the ultrahigh vacuum (UHV) setup, the specially designed segmented linear ion trap, the optical setup as well as the extraction mechanism and the utilized ion optics. In section 3, we present the experimental results, namely the deterministic loading of single $^{40}Ca^{+}$ ions and the focusing of the single-ion beam to a 5 μm spot. Finally, in section 4, we give a short conclusion and sketch possible future applications.

2. Experimental set-up

2.1. UHV set-up

The core piece of the UHV set-up is a Magdeburg hemisphere from Kimball Physics[4] with an inner diameter of 91.5 mm and a total length of 106 mm. It features a total of seven different access ports with flange sizes ranging from DN16CF to DN63CF. A specifically designed segmented linear ion trap (see section 2.2) is mounted inside the hemisphere with the trap axis being located 165 mm above the optical table.

All access ports are equipped with fused silica (SiO_2) windows, allowing for optical access with laser beams and for imaging the ions. A 20-pin vacuum feedthrough for the dc electrodes and the ovens is connected via a T-piece to the hemisphere, whereas the power supply for the rf electrodes is managed using a separate 4-pin vacuum feedthrough, which is mounted on a four-way cross, see also figure 1. Using an all-metal gate valve from VAT[5], the main vacuum chamber is connected to a separate detector chamber, which is attached to a specifically designed translation stage. In combination with a membrane below, the translation stage allows for rotating the detector chamber in the horizontal and vertical directions with respect to the trapping position of the ion, compensating for any misalignment between the trap axis and the optical axis of the utilized ion optics. The complete set-up measures 850 mm in length with a depth of 480 mm and a total height of about 380 mm. The pressure is held by a 20 litre s^{-1} VacIon *Plus* StarCell ion getter pump and a titanium sublimation pump[6]. In addition, both the main vacuum and the detector chamber are connected via all-metal angle valves to a turbo-molecular pump from Oerlikon[7]. The base pressure of the UHV set-up equals 5×10^{-10} mbar, which is measured using a Varian UHV-24p Bayard-Alpert-type ionization gauge tube.

2.2. Segmented linear rail trap

The trap consists of four copper-plated polyimide blades, which were manufactured using printed circuit board (PCB) technology and are arranged in an X-shaped manner [22]. It features a total of 15 independent dc electrodes, which can be assigned to three different trap sections: a wide loading zone (electrodes 1–4) is connected via a taper (electrode 5) to a narrow

[4] Kimball Physics Inc., USA.
[5] VAT Deutschland GmbH, Germany.
[6] Varian Inc., USA.
[7] Oerlikon Leybold Vacuum GmbH, Germany.

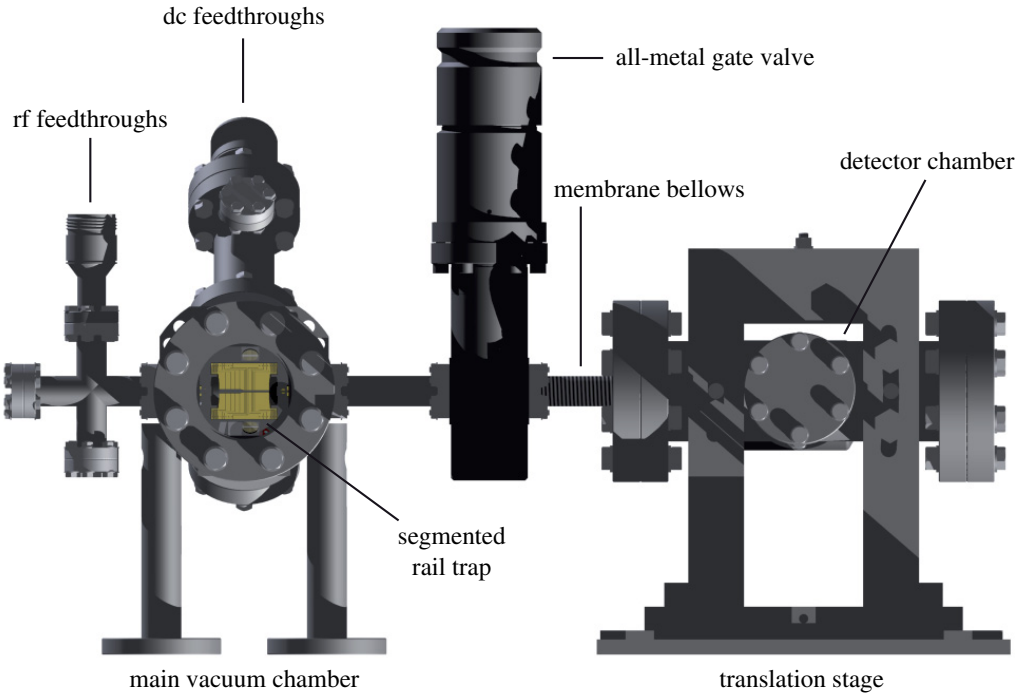

Figure 1. Schematic drawing of the UHV set-up. The set-up consists of a main vacuum chamber and a detector chamber, which are connected via an all-metal gate valve. A membrane below in combination with a specifically designed translation stage allows for rotating the detector chamber in the horizontal and vertical directions with respect to the trapping position of the ion.

experimental zone (electrodes 6–14). A deflection electrode (electrode 15) is used to alter the trajectories of ions that are extracted out of the trap. In order to generate the radial confinement, an additional electrode runs along the inner front face of each blade, which will be referred to as a rail in the following. The blade itself has a total length of 65 mm and a thickness of 410 μm with 18 μm copper plating on both sides. Electrodes 2–5 as well as electrode 14 have a width of 2.8 mm, and electrodes 6–13 have a width of 0.7 mm. In order to efficiently deflect ions by targeted application of low voltages, the deflection electrode has been elongated in the extraction direction, featuring a total length of 20.6 mm. The distance between the rf rail and the dc electrodes as well as between adjacent dc electrodes equals 0.1 mm (see also figure 2 for a technical drawing of one of the four trap blades).

The distance between the inner front faces of opposing blades equals 4 mm in the loading zone and 2 mm in the experimental zone. In the case of a standard Paul trap, the rf voltage is supplied to two of the four blades. The other two blades are used for the axial confinement and are therefore divided into several electrodes. However, in the case of our rail trap, all four blades are identical. Apart from the deflection electrodes, the corresponding electrodes on all four blades (i.e. electrode 1 of each of the blades) are electrically connected together, resulting in a stronger and more symmetrical axial confinement than in the standard case. The rf voltage is only applied to the rails of two opposing blades; the front faces of both of the other blades are grounded, generating the quadrupole potential for the radial confinement. As these rails run along the whole trap axis and continue around the corner at the end of each blade, the

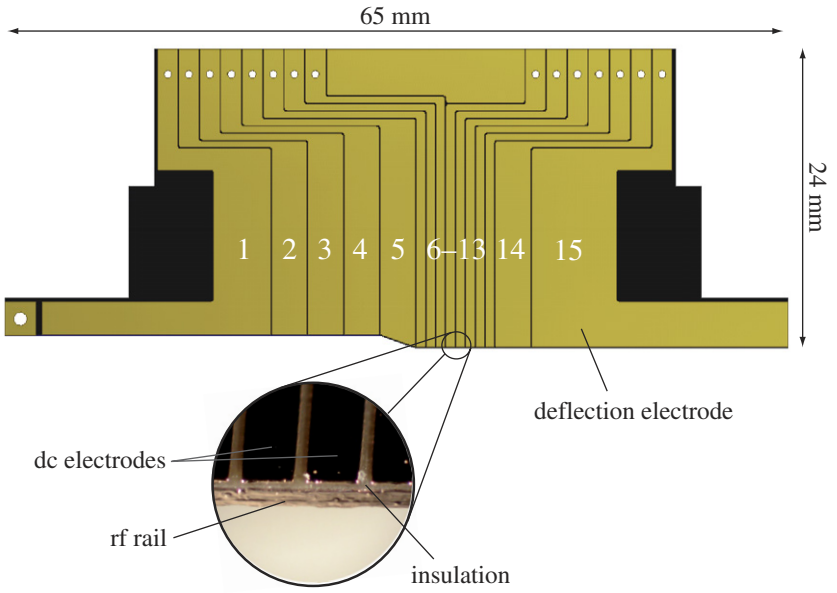

Figure 2. Technical drawing of one of the four trap blades featuring a total of 15 independent dc electrodes. A wide loading zone (electrodes 1–4) is connected via a taper (electrode 5) to a narrow experimental zone (electrodes 6–14). A deflection electrode (electrode 15) is used to alter the trajectories of the extracted ions. The rf rail has a thickness of about 22 μm and covers the whole front of the blade. Isolated parts are colored black. The close-up view shows a microscope image of the front part of the blade.

radial confinement is sustained during the whole extraction process and targeted shooting is accomplished.

Under typical operating conditions, we apply a voltage of 400 V_{pp} at a frequency of $\Omega/2\pi = 12.155$ MHz to the rf electrodes, leading to a radial secular frequency $\omega_{rad}/2\pi = 430$ kHz for a $^{40}Ca^{+}$ ion. The dc-electrode trap segments 7 and 13 are supplied with 35 V and the remaining electrodes with 0 V, resulting in an axial trapping potential with $\omega_{ax}/2\pi = 280$ kHz. The location of trapped ions is above electrode 10.

2.3. Optical set-up

The generation of the necessary laser beams is mainly done by using commercial grating stabilized diode laser systems from TOPTICA[8]. The ions are illuminated by resonant laser light near 397 and 866 nm for Doppler cooling. Scattered photons are collected by an $f/1.76$ lens on an EMCCD camera[9] to image individual $^{40}Ca^{+}$ ions. From the width of the laser excitation spectrum on the $S_{1/2}$–$P_{1/2}$ laser cooling transition, we deduce a temperature of about 2 mK, slightly above the Doppler cooling limit. Calcium and dopant ions are generated in a multi-photon ionization process by a pulsed frequency tripled Nd-YAG laser at 355 nm with a pulse power of 7 mJ. Dopant ions are sympathetically cooled and identified from the voids in the

[8] TOPTICA Photonics AG, Germany.
[9] Andor Technology, model DV885KCS-VP.

fluorescence image compared to that of a regular linear $^{40}Ca^{+}$ crystal. The species of dark ions can be identified by exciting collective vibrational modes with an ac voltage applied to electrode 9 and observing a blurring of the $^{40}Ca^{+}$ fluorescence image at the resonance frequency $\omega_{ax.}$ [23]. Alternatively, amplitude-modulated resonant laser light is used [24] to determine the charge-to-mass ratio of trapped particles at a precision of better than 0.2%. In order to suppress vibrations of the building and to reduce thermal elongations to a minimum, the complete set-up is located on an air-suspended optical table that is situated in a temperature-stabilized laboratory.

2.4. Extraction mechanism and set-up

Initially, the ion is trapped at the center of electrode 10 by supplying a voltage of 35 V to electrodes 7 and 13 (see also figure 5(a) for a simulation of the trapping potential in the axial direction). However, due to the distance from the electrodes to the trap center, the generated axial trapping potential only features a depth of about 4 eV, not representing a large barrier during the extraction process. The extraction process is then initiated by increasing the dc voltages on electrodes 9 and 10 to 500 V within a few tens of nanoseconds. The extraction voltage generates a repulsive potential at the position of the ion, effectively canceling the axial confinement. However, as the ion already gets accelerated by the developing potential during the switching process, the ion does not sense the full potential strength and the effective energy transfer is lessened. In addition, due to the asymmetric voltage configuration, the peak voltage is not at the position of the ion and it is only accelerated by the shoulder of the generated potential, reducing the kinetic energy even further. From a time-of-flight analysis, one can deduce a final kinetic energy of about 80 eV for the extracted $^{40}Ca^{+}$ ions [20].

Figure 3 shows a schematic drawing of the extraction set-up. After a specified number of ions has been loaded into the trap (in this case, a linear ion crystal consisting of four $^{40}Ca^{+}$ ions), the extraction process is triggered via a computer-controlled TTL signal that is fed in a phase synchronization circuit (phase delay trigger). The phase synchronization circuit delays the TTL signal such that a constant delay to the next zero crossing of the trap drive frequency Ω is ensured as the synchronization is crucial in order to minimize shot-to-shot fluctuations of the velocity and position of the extracted ions. The measured delay time shows a 1σ-spread of 0.34 ns. The switching of the extraction voltage[10] is experimentally realized by two high voltage switches[11], which can switch voltages of up to 4 kV within a time span of 20 ns. However, as the extraction voltage leads to a temporary charging of the trap, the TTL trigger signal is supplied for only a few milliseconds to the high-voltage switches, reducing the unintentional charging to a minimum.

The detection of the extracted ions is then performed via an electron multiplier tube (EMT)[12] with 20 dynodes and a main entrance aperture of 20 mm that can detect positively charged ions with a specified quantum efficiency of about 80% and a specified gain of 5×10^5. Under typical operating conditions, the detector is supplied with a voltage of -2.5 kV, leading to detection signals with a width of 10–15 ns and an amplitude of about 100 mV, which are recorded via an oscilloscope[13]. As already stated in section 2.1, the detector is housed in a separate vacuum chamber with a distance of 287 mm from the trap center.

[10] ISEC Inc., model EHQ-8010p.
[11] Behlke Inc., model HTS 41-06-GSM.
[12] ETP Inc., model AF553.
[13] Agilent Infiniium 54832D MSO.

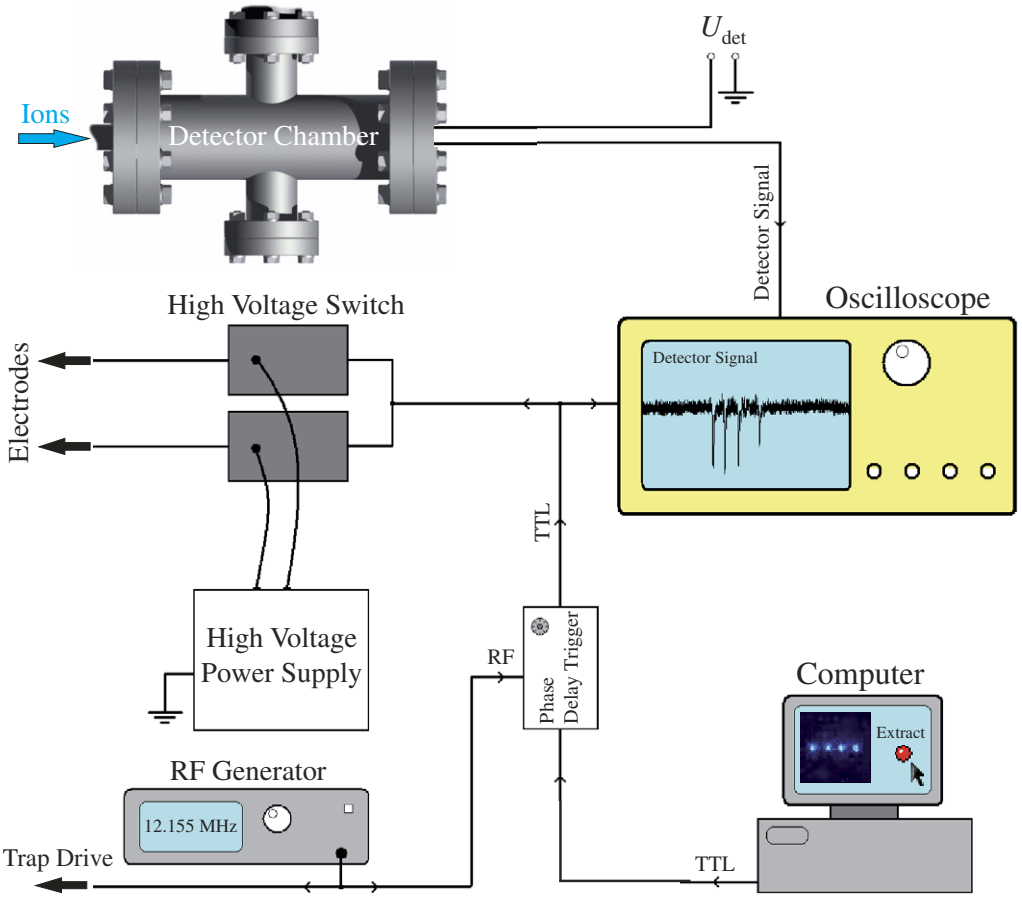

Figure 3. Schematic drawing of the extraction set-up. After a certain number of ions have been loaded into the trap, the extraction process is triggered via a TTL signal that is synchronized to the trap drive frequency Ω using a phase synchronization circuit (phase delay trigger). Two high-voltage switches then increase the dc voltages on electrodes 9 and 10 to 500 V within a few tens of nanoseconds, leading to the extraction of the trapped ions. Upon entering the detector chamber, the extracted ions are detected using an electron multiplier tube, leading to signal dips on an oscilloscope.

2.5. Ion optics

The utilized einzel lens consists of three stainless steel electrodes that feature an outer diameter of 27 mm. The first electrode has a thickness of 0.2 mm with an inner diameter of 8 mm, and the second electrode has a thickness of 0.4 mm and an inner diameter of 8 mm. The third electrode consists of two parts: the first part is a cylindrical-shaped spacer with an inner diameter of 16 mm and a thickness of 4.95 mm, whereas the second part consists of a stainless steel plate with a thickness of 1 mm featuring a 4 mm aperture that is also used as a mounting for all the other electrodes. The first and third electrodes are conductively interconnected, whereas the second electrode is electrically insulated by using Kapton sheets with a thickness of 0.05 mm (see also figure 4(a) for a schematic drawing of the einzel lens). The calculation of the electrostatic

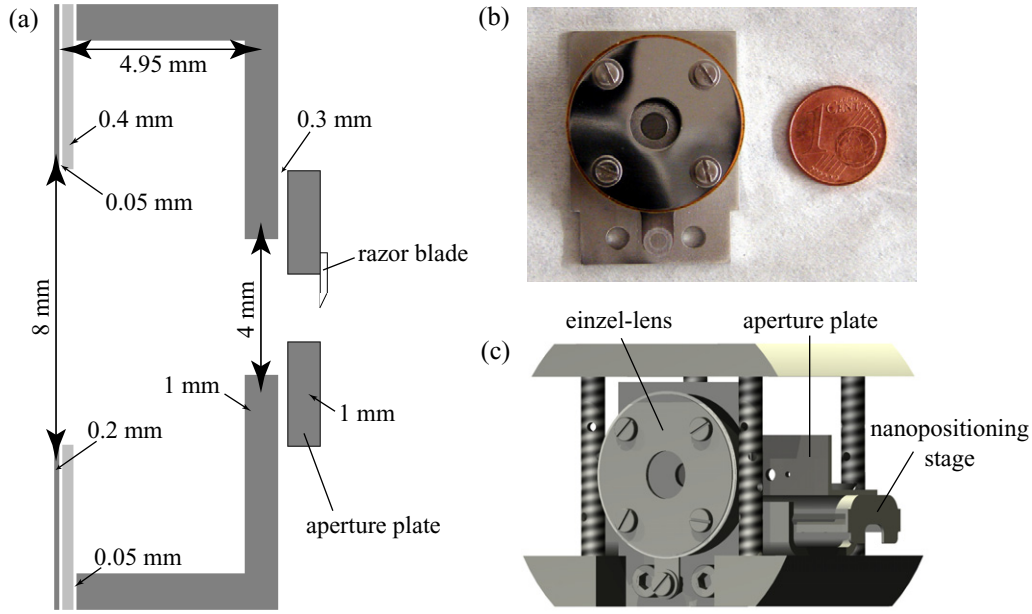

Figure 4. (a) Schematic drawing of the einzel lens with the dc electrode depicted in light grey and grounded electrodes colored dark grey. The razor blade (depicted in white), which is mounted behind the 2 mm aperture of the movable aperture plate, is also included. (b) Picture of the assembled einzel lens, with a one-cent coin for size comparison. Under typical operating conditions, the dc electrode is supplied with a voltage of 150 V. (c) Schematic drawing of the einzel lens and the nanopositioning stage, which are located at the beginning of the detector chamber directly in front of the EMT.

potentials of the einzel lens and the ion ray tracing simulations are performed by a high-accuracy boundary-element solver package [25]. A detailed description of the imaging characteristics for different types of lens configurations can be found in [26].

All parts are electropolished in order to remove ridges that were formed during the manufacturing process and to reduce the overall surface roughness. For electropolishing, we use a solution of phosphoric acid (H_3PO_4), methanesulfonic acid (CH_3SO_3H) and triethanolamine ($C_6H_{15}NO_3$).[14] The parts are polished for a timespan of 15 min at a temperature of 65 °C using an anodic current density of 5 A dm^{-2}. Figure 4(b) shows a picture of the assembled einzel lens, with a one-cent coin for size comparison. Under typical operating conditions, the second electrode of the einzel lens is supplied with a voltage of 150 V, whereas the other two electrodes are grounded.

In order to determine the diameter of the single-ion beam, a movable aperture plate is installed between the einzel lens and the detector, featuring hole diameters ranging from 5 mm down to 300 μm. In addition, a razor blade is attached behind the 2 mm aperture, effectively creating a well-defined tearing edge (see also figure 4(a) and section 3.2). The plate is mounted on a nanopositioning stage[15], which allows the aperture plate to be moved with an accuracy of

[14] Patent specification DE102006050317B3.
[15] SmarAct, model SL-2040.

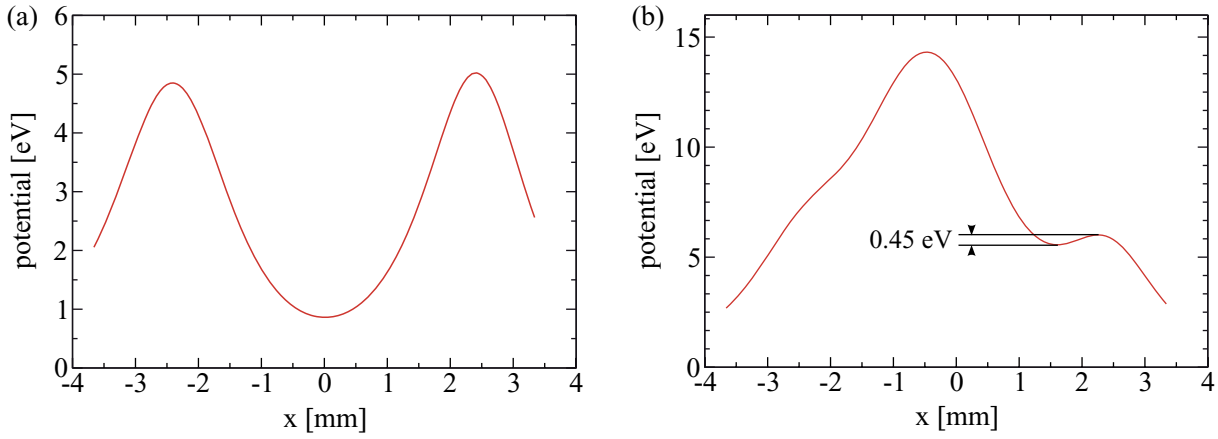

Figure 5. (a) Simulated trapping potential in the axial direction. The potential is generated by supplying dc electrodes 7 and 13 with a voltage of 35 V and all the remaining electrodes with 0 V, resulting in an axial trapping frequency $\omega_{\text{ax.}} = 2\pi \times 280$ kHz and a trap depth of about 4 eV. The center of electrode 10 is used as the point of reference for the axial position. (b) The same potential as in (a) but with a voltage of 54.8 V applied to electrodes 9 and 10, reducing the axial trap depth to about 0.45 eV in order to get rid of the surplus ions.

a few tens of nanometers. An internal sensor module guarantees that the absolute position of the stage is kept constant. Figure 4(c) shows a schematic drawing of the einzel lens and the nanopositioning stage, which are located at the beginning of the detector chamber directly in front of the EMT.

3. Experimental results

3.1. Deterministic single-ion loading

In order to reduce the divergence of the ion beam to a minimum, it is necessary to ensure that only one ion is extracted out of the trap with each shot. In the case of a Paul trap, there are, in principle, two options to achieve this goal. The first option is to avoid the loading of more than one ion at a time. Since this is not feasible due to the fact that the number of loaded ions follows a Poissonian distribution for equal loading times, one needs to implement a feedback control in order to stop the ionization after one ion has been loaded into the trap. As it turned out, it was not possible to implement this method in our set-up as the time that elapses between the ionization and crystallization of a one-ion crystal has to be much shorter than the average time between ionization incidents of two different ions. Therefore, we have chosen the second possibility, namely to get rid of the redundant ions after the crystallization process. For this task, we have come up with a very simple and robust procedure that is described next.

To drop the surplus ions, we exploit the potential shaping capabilities offered by our segmented linear rail trap (see also section 2.2). At the beginning, the ions are trapped above electrode 10 by supplying a voltage of 35 V to electrodes 7 and 13, leading to an axial trapping potential with a trap depth of about 4 eV (see also figure 5(a)). By using the offset input of our high-voltage switches (see also section 2.4), the voltage supplied to electrodes 9 and 10 is

linearly ramped up from 0 to 54.8 V within a timespan of about 50 ms before it is again linearly reduced to 0 V after a waiting time of 200 ms. As a consequence, the depth of the axial trapping potential is reduced to about 0.45 eV, thus becoming shallow enough that only one ion will remain inside the trap (see also figure 5(b)). In order to determine the reproducibility of our method, we repeated the procedure described above with ion crystals of various sizes, yielding a total efficiency of 96.7(7)% for reducing the amount of ions to exactly one. By means of this approach, it is also possible to reduce the number of ions in the chain to an arbitrary predefined quantity, e.g. from 5 to 4 ions, but since this is not used for the experiments below, we do not discuss it any further.

3.2. Experimental determination of the spot size

In former measurements, we determined the size of our ion beam by shooting single ions through the 300 μm aperture, yielding a spot radius of $83(^{+8}_{-3})$ μm and a full-angle beam divergence of 600 μrad at a distance of 257 mm from the trap center [20]. Here, 68.3% of all detected ions were located inside the stated spot radius. However, in order to compare these values with our current measurements, we converted them according to equation (1), resulting in a 1σ-spot radius of $55(^{+5}_{-2})$ μm. To further improve the resolution of our single-ion beam, we installed an einzel lens between the trap and the detector (see also section 2.5). In order to obtain an optimal alignment with respect to the optical axis of the einzel lens, the radial adjustment of the ion beam is performed by utilizing the deflection electrodes of our segmented rail trap. Using the 1 mm aperture behind the einzel lens, the optimal deflection voltages are retrieved by gradually changing them, maximizing the hit rate on the detector. As it turns out, the hit rate is very sensitive to changes of the deflection and compensation voltages, i.e. a minor change in the range of a few millivolts is already sufficient to miss the 1 mm aperture, effectively reducing the measured hit rate to zero. Hence, to keep adjacent measurements consistent with each other, all the measurements presented were conducted with a fixed set of deflection and compensation voltages.

In order to determine the spot size of the ion beam in the focal plane of the installed ion optics, we utilize the aforementioned razor blade that is mounted behind the 2 mm aperture (see also section 2.5). By moving the razor blade stepwise into the path of the generated single-ion beam, a gradual cut-off of the ion trajectories is achieved, leading to a reduction in the overall hit rate on the detector. To derive the 1σ-spot radius, these points are then fitted with an error function, which itself is obtained by integrating a Gaussian distribution that will be assumed for the radial cross-section of the single-ion beam:

$$f(x) = \int_{-\infty}^{x} \frac{c}{\sigma\sqrt{2\pi}} \exp\left[-\frac{1}{2}\left(\frac{y-a}{\sigma}\right)^2\right] \mathrm{d}y = \frac{c}{2}\left(1 + \mathrm{erf}\left(\frac{x-a}{\sigma\sqrt{2}}\right)\right). \qquad (1)$$

Here, σ denotes the radius of the ion beam with a being the offset in the x-direction. The parameter c is used as a scaling factor in order to account for the detector efficiency, which has been experimentally measured to be 0.87 [20]. As the timespan needed for doing a single measurement is considerably long ($\approx$3 incidents per minute), we had to reduce the number of measurements taken for each blade position to a total of ten individual shots. This was done in order to avoid changes in the deflection and compensation voltages, which would have been necessary to counteract long-term drifts caused by a thermal expansion of the trap.

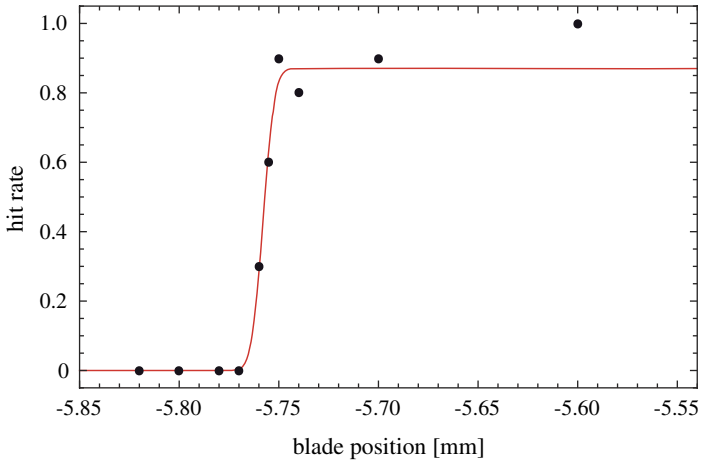

Figure 6. Experimental determination of the spot size. The graph shows the hit rate for single ions as a function of the blade position for a lens voltage of 150 V, resulting in a 1σ-spot radius of $(4.6 \pm 1.3)\ \mu$m.

Because the exact focal distance of our einzel lens is unknown, one would normally have to repeat the measurement described above for different spacings between the einzel lens and the razor blade. However, as our nanopositioning stage is only capable of moving perpendicular to the ion beam, the location of the focal plane of the einzel lens has to be adjusted by changing the lens voltage. Measuring the spot radius for different lens voltages in the plane of the razor blade, therefore, should allow for obtaining the minimal spot radius. In the experiment, we have measured a 1σ-spot radius of $(4.6 \pm 1.3)\ \mu$m for a lens voltage of 150 V (see also figure 6). Compared to the original beam diameter, our einzel lens is thus capable of focusing the single-ion beam by a factor of 12.

Numerical simulations predict that an even higher resolution should be feasible. In the case of ground-state cooled ions with a temperature of 100 μK, simulations predict a 1σ-spot radius of 1 nm, which is enlarged to 45 nm for a temperature of 2 mK. However, in the experiment, additional deflection voltages are needed in order to align the ion beam with respect to the optical axis of the utilized einzel lens. Including these deflection voltages in the numerical simulations leads to a further decline in resolution, resulting in a 1σ-spot radius of about 270 nm. Only taking into account a spatial displacement of the incident ion beam in the principal plane of the lens, numerical simulations predict that a mismatch of 520 μm with respect to the optical axis is already sufficient in order to obtain a spot size of 4.6 μm in the focal plane of the lens (see also figure 7). In the case of our experiment, this displacement is caused by a mechanical misalignment of the center of the aperture with respect to the optical axis of the einzel lens, as well as a displacement of the ion beam itself within the 1 mm aperture. The former can be ascribed to manufacturing imperfections, which are estimated to be about 200 μm. The latter is caused by the initial adjustment of the ion beam using the 1 mm aperture. By taking into account the original beam diameter, a displacement of less than 400 μm can be assumed. Hence, both errors result in a maximum total deviation of 600 μm, explaining the numerically predicted mismatch. A more compact experimental set-up as compared with the total length of about 260 mm (see figure 1) is envisioned for the future.

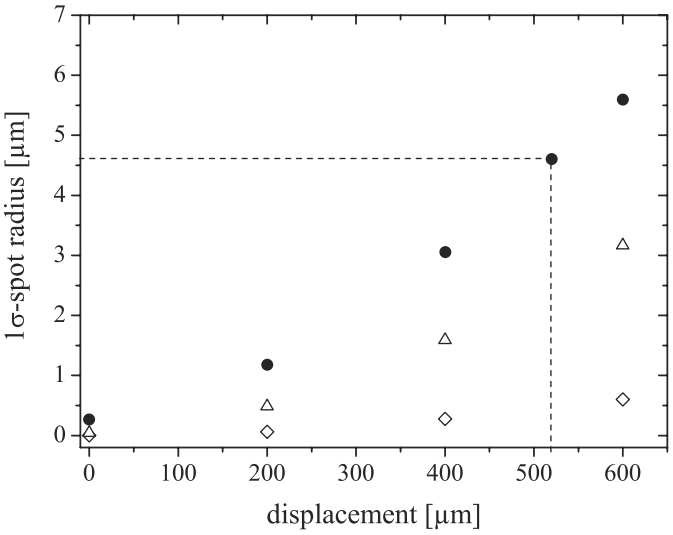

Figure 7. Simulated 1σ-spot radii as a function of the spatial displacement of the ion beam in the principal plane of the lens. The radii were calculated for an initial ion temperature of 2 mK with (●) and without (△) deflection voltages as well as for an initial ion temperature of 100 μK without deflection voltages (◇). In order to explain the experimentally measured 1σ-spot radius of 4.6 μm for 2 mK laser-cooled ions, a displacement of half a millimeter is already sufficient (dashed lines). Note that the initial ion temperature and deflection voltages for the simulated dataset (●) match the experimental conditions, whereas the spatial displacement was not determined experimentally.

4. Conclusion and outlook

Using a segmented linear Paul trap as a deterministic point source for laser-cooled ions, we have demonstrated the focusing of an ion beam consisting of single $^{40}Ca^{+}$ ions to a spot size of a few micrometers. By utilizing the potential shaping capabilities of our ion trap, we were able to deterministically load a predetermined number of ions, which will allow for further automatization of the loading and extraction procedure, resulting in orders of magnitude increased repetition rates. In future experiments, efforts will be made to avoid the usage of the deflection electrodes by aligning the beam mechanically and to implement more sophisticated cooling techniques like side band or EIT cooling in order to reduce the divergence of the ion beam. Moreover, the utilized nanopositioning stage will be exchanged for a modular set-up consisting of three independent stages in order to move apertures and substrates in all three spatial directions. The additional degrees of freedom will not only allow for a more precise alignment with respect to the optical axis of the einzel lens but also allow us to determine the optimal focal length and spot size more accurately. Using two perpendicular edges of the substrate in the same way as the razor blade will then allow for approaching a specific location on the substrate relative to the corner formed by the two edges. Alternatively, one could think of mounting the einzel lens on the tip of an AFM, thus allowing for determining the implantation position with respect to potential surface structures [21]. A new lens design, which is currently in development, will facilitate better focusing of the single-ion beam and additionally allow for

post-accelerating the extracted ions in order to reach higher implantation energies of a few keV, i.e. improving the conversion efficiency for the generation of color centers in diamond [27]. Due to the high spatial and temporal resolution of the focused single-ion beam, one might also consider shooting ions from one ion trap into another. This would allow us to transport quantum information stored in the internal, electronic states of the ions much more quickly and over larger distances than currently possible when performing standard ion transport in multi-segmented micro ion traps.

Acknowledgments

We acknowledge the financial support of the Landesstiftung Baden–Württemberg in the framework of 'Atomics' (contract no. PN 63.14) and the excellence program.

References

[1] Gurudev Dutt M V, Childress L, Jiang L, Togan E, Maze J, Jelezko F, Hemmer P R, Zibrov A S and Lukin M D 2007 Quantum register based on individual electronic and nuclear spin qubits in diamond *Science* **316** 1312

[2] Neumann P, Mizuochi N, Rempp F, Hemmer P, Watanabe H, Yamasaki S, Jacques V, Gaebel T, Jelezko F and Wrachtrup J 2008 Multipartite entanglement among single spins in diamond *Science* **320** 1326

[3] Kane B E 1998 A silicon-based nuclear spin quantum computer *Nature* **393** 133

[4] Greentree A D, Fairchild B A, Hossain F M and Prawer S 2008 Diamond integrated quantum photonics *Mater. Today* **11** 22

[5] Shinada T, Koyama H, Hinishita C, Imamura K and Ohdomari I 2002 Improvement of focused ion-beam optics in single-ion implantation for higher aiming precision of one-by-one doping of impurity atoms into nano-scale semiconductor devices *Japan. J. Appl. Phys.* **41** L287

[6] Persaud A, Park S J, Liddle J A, Rangelow I W, Bokor J, Keller R, Allen F I, Schneider D H and Schenkel T 2004 Quantum computer development with single ion implantation *Quantum Inf. Process.* **3** 233

[7] Mitic M *et al* 2005 Single atom Si nanoelectronics using controlled single-ion implantation *Microelectron. Eng.* **78–79** 279

[8] Batra A, Weis C D, Reijonen J, Persaud A, Schenkel T, Cabrini S, Lo C C and Bokor J 2007 Detection of low energy single ion impacts in micron scale transistors at room temperature *Appl. Phys. Lett.* **91** 193502

[9] Shinada T, Kurosawa T, Nakayama H, Zhu Y, Hori M and Ohdomari I 2008 A reliable method for the counting and control of single ions for single-dopant controlled devices *Nanotechnology* **19** 345202

[10] O'Brien J L, Schofield S R, Simmons M Y, Clark R G, Dzurak A S, N J, Curson Kane B E, McAlpine N S, Hawley M E and Brown G W 2001 Towards the fabrication of phosphorus qubits for a silicon quantum computer *Phys. Rev.* B **64** 161401

[11] Schofield S R, Curson N J, Simmons M Y, Ruess F J, Hallam T, Oberbeck L and Clark R G 2003 Atomically precise placement of single dopants in Si *Phys. Rev. Lett.* **91** 136104

[12] Ruess F J, Oberbeck L, Simmons M Y, Goh K E J, Hamilton A R, Hallam T, Schofield S R, Curson N J and Clark R G 2004 Toward atomic-scale device fabrication in silicon using scanning probe microscopy *Nano. Lett.* **4** 1969

[13] Pok W, Reusch T C G, Scappucci G, Rueb F J, Hamilton A R and Simmons M Y 2007 Electrical characterization of ordered Si:P dopant arrays *Trans. IEEE. Nanotechnol.* **6** 213

[14] Ruess F J, Pok W, Reusch T C G, Butcher M J, Goh K E J, Scappucci G, Hamilton A R and Simmons M Y 2007 Realization of atomically controlled dopant devices in silicon *Small* **3** 563

[15] Greiner A, Sebastian J, Rehme P, Aghajani-Talesh A, Griesmaier A and Pfau T 2007 Loading chromium atoms in a magnetic guide *J. Phys. B: At. Mol. Phys.* **40** F77

[16] Hill S B and McClelland J J 2003 Performance of a feedback-controlled, deterministic source of single chromium atoms *J. Opt. Soc. Am.* B **21** 473
[17] Hanssen J L, McClelland J J, Dakin E A and Jacka M 2006 Laser-cooled atoms as a focused ion-beam source *Phys. Rev.* A **74** 063416
[18] Hanssen J L, Hill S B, Orloff J and McClelland J J 2008 Magneto-optical-trap-based, high brightness ion source for use as a nanoscale probe *Nano Lett.* **8** 2844
[19] Meijer J *et al* 2006 Concept of deterministic single ion doping with sub-nm spatial resolution *Appl. Phys.* A **83** 321
[20] Schnitzler W, Linke N M, Fickler R, Meijer J, Schmidt-Kaler F and Singer K 2009 Deterministic ultracold ion source targeting the Heisenberg limit *Phys. Rev. Lett.* **102** 070501
[21] Meijer J *et al* 2008 Towards the implanting of ions and positioning of nanoparticles with nm spatial resolution *Appl. Phys.* A **91** 567
[22] Huber G, Deuschle T, Schnitzler W, Reichle R, Singer K and Schmidt-Kaler F 2008 Transport of ions in a segmented linear Paul trap in printed-circuit-board technology *New J. Phys.* **10** 013004
[23] Naegerl H, Blatt R, Eschner J, Schmidt-Kaler F and Leibfried D 1998 Coherent excitation of normal modes in a string of Ca^+ ions *Opt. Express* **3** 89
[24] Drewsen M, Mortensen A, Martinussen R, Staanum P and Sørensen J L 2004 Nondestructive identification of cold and extremely localized single molecular ions *Phys. Rev. Lett.* **93** 243201
[25] Singer K, Poschinger U, Murphy M, Ivanov P, Ziesel F, Calarco T and Schmidt-Kaler F 2009 Colloquium: experiments with atomic quantum bits—essential numerical tools arXiv:0912.0196
[26] Fickler R, Schnitzler W, Linke N M, Schmidt-Kaler F and Singer K 2009 Optimized focusing ion optics for an ultracold deterministic single ion source targeting nm resolution *J. Mod. Opt.* **56** 2061
[27] Jelezko F and Wrachtrup J 2006 Single defect centres in diamond: a review *Phys. Status Solidi* a **203** 3207